

Reachability Constrained Reinforcement Learning

Dongjie Yu^{*1} Haitong Ma^{*1} Shengbo Eben Li¹ Jianyu Chen^{2,3}

Abstract

Constrained Reinforcement Learning (CRL) has gained significant interest recently, since the satisfaction of safety constraints is critical for real world problems. However, existing CRL methods constraining discounted cumulative costs generally lack rigorous definition and guarantee of safety. On the other hand, in the safe control research, safety is defined as persistently satisfying certain state constraints. Such persistent safety is possible only on a subset of the state space, called feasible set, where an optimal largest feasible set exists for a given environment. Recent studies incorporating safe control with CRL using energy-based methods such as control barrier function (CBF), safety index (SI) leverage prior conservative estimation of feasible sets, which harms performance of the learned policy. To deal with this problem, this paper proposes a reachability CRL (RCRL) method by using reachability analysis to characterize the largest feasible sets. We characterize the feasible set by the established self-consistency condition, then a safety value function can be learned and used as constraints in CRL. We also use the multi-time scale stochastic approximation theory to prove that the proposed algorithm converges to a local optimum, where the largest feasible set can be guaranteed. Empirical results on different benchmarks such as safe-control-gym and Safety-Gym validate the learned feasible set, the performance in optimal criteria, and constraint satisfaction of RCRL, compared to state-of-the-art CRL baselines.

1. Introduction

Constrained Reinforcement learning (CRL) has gained growing attention due to safety requirements in the practical

^{*}Equal contribution ¹School of Vehicle and Mobility, Tsinghua University, Beijing, China ²Institute for Interdisciplinary Information Sciences, Tsinghua University, Beijing, China ³Shanghai Qizhi Institute, Shanghai, China. Correspondence to: Shengbo Eben Li <lishbo@tsinghua.edu.cn>.

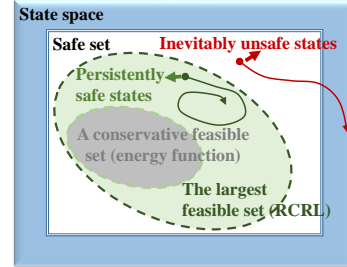


Figure 1. The intuitive relationship among the state space, safe states, feasible sets and the largest feasible set.

applications of RL. The safety specifications in common CRL methods are expected discounted cumulative costs (Altman, 1999; Achiam et al., 2017; Tessler et al., 2019; Yang et al., 2020). However, the main deficiency of this design is averaging the potential danger at a specific state to the whole trajectory. For example, the autonomous vehicle should always keep a safe distance to other traffic participants but not keep the cumulative or average distance during a period where the collision might happen at a single time step. Therefore, the discounted cumulative costs design lacks rigorous definition and guarantee of safety.

Meanwhile, the persistent state constraint satisfaction in the safe control research clarifies how to characterize the safety of states with rigorous definitions (Liu & Tomizuka, 2014; Ames et al., 2019; Choi et al., 2021). Rich theoretical and practical techniques for ensuring safety in such settings are provided, where an important fact is that only a subset of states can be guaranteed safe persistently, called feasible set. Outside of this set, even temporally safe states will violate the constraints inevitably in the future, no matter what policies to choose, as shown in Figure 1. For example, if a vehicle is too close to a front obstacle with high speed, it is doomed to crash since the deceleration capability is limited. Therefore, accurately identifying feasible sets in CRL can significantly affect the performance and safety of the learned policy.

Some recent studies adopt energy-based methods to consider persistent safety and feasible sets in RL. Representatives include control barrier function (CBF) (Ames et al., 2019; Ma et al., 2021a) and safety index (SI) (Liu & Tomizuka, 2014; Ma et al., 2021c). However, these methods rely on prior specifications of the energy function, which result in conser-

vative feasible sets (as Figure 1 shows), causing unsatisfying performance sacrifice. Hamilton-Jacobi (HJ) reachability analysis is another branch in the safe control research, which identifies the theoretical largest feasible set (Lygeros et al., 1999; Mitchell et al., 2005; Bansal et al., 2017). Recently some pioneering studies migrated HJ reachability analysis to model-free RL (Fisac et al., 2019; Hsu et al., 2021). However, these works obtain only the safest policies, leaving the performance criterion (e.g., reward optimization) unconsidered. This safety-only design significantly limits broader applications of HJ reachability analysis in RL.

This paper proposes reachability constrained reinforcement learning (RCRL), which learns the optimal policy satisfying persistent safety within the identified largest feasible set. RCRL introduces a novel constraint imposed on the safety value function, which is a critical notion in HJ reachability analysis. Intuitively speaking, it describes the worst constraint-violation in the long term, and its sub-zero level set is the feasible set. We derive a self-consistency condition of the safety value function and incorporate it into the CRL framework. We use the multi-time scale stochastic approximation theory (Borkar, 2009; Chow et al., 2017) to prove that the proposed algorithm converges to a local optimum where the largest feasible set can be guaranteed, as shown in Figure 1. Empirical results on low-dimensional problems validate the correctness of the learned feasible sets. Further experiments conducted on complex benchmarks such as safe-control-gym (Yuan et al., 2021) and Safety-Gym (Achiam & Amodei, 2019) indicate that RCRL achieves near-optimal performance while maintaining constraint-satisfaction. Our main contributions are:

- We are the first to introduce reachability constraints into CRL, which is critical for learning a nearly optimal and persistently safe policy upon the largest feasible set. The largest feasible set can be identified through the established self-consistency condition, avoiding the time-consuming calculation of the safest policy faced by conventional HJ approaches.
- We use the multi-time scale stochastic approximation theory to prove that RCRL converges to a locally optimal policy, which also persistently satisfies the state constraints across the entire largest feasible set.
- Comprehensive experiments demonstrate that the proposed RCRL method outperforms state-of-the-art CRL baselines in terms of both final performance and constraint satisfaction.

2. Related Work

Constrained Reinforcement Learning (CRL) is an active research area in safe RL aiming to learn effective and safe

policies for sequential decision-making tasks. CRL problems is usually formulated as constrained Markov decision process (CMDP) (Altman, 1999; Brunke et al., 2021). Constrained optimization approaches are adopted to solve CRL problems: 1) penalty function (Guan et al., 2021b); 2) Lagrangian methods (Tessler et al., 2019; Chow et al., 2017; Duan et al., 2021b; Ma et al., 2021b) and 3) trust-region methods (Achiam et al., 2017; Yang et al., 2020). CRL works based on CMDP rely on the expected discounted cumulative costs and a hand-crafted threshold to improve the safety of policies. However, a proper threshold relies on engineering intuition and varies in different tasks (Qin et al., 2021). In other words, the crucial feasible sets cannot be defined rigorously and generally under this setting.

Characterizing Feasible Sets is a critical and open problem in the safe control research (Brunke et al., 2021). The feasible set is always represented by a safety certificate. Some methods propose energy function such as CBF (Ma et al., 2021a; Choi et al., 2021) and SI (Liu & Tomizuka, 2014) as the certificate. The core idea is that the dynamical system is approaching the safer region when its energy dissipates (Ames et al., 2019). Nevertheless, the energy-based methods lack generality and suffer from conservativeness (Ma et al., 2021c). HJ reachability analysis is a promising way towards general and rigorous derivation of feasible sets (Lygeros et al., 1999; Mitchell et al., 2005). However, it is quite difficult to solve the largest feasible set because it is represented by a partial differentiable equation, whose analytical solution is generally intractable to solve (Bansal et al., 2017). Machine learning especially RL approaches are adopted to deal with this problem (Fisac et al., 2019; Bansal & Tomlin, 2021; Hsu et al., 2021). However, they care only about safety while ignoring other metrics, especially the optimality criterion. This limits reachability analysis approaches to broader applications. Therefore, to the best of our knowledge, this is the first work to characterize the feasible set in CRL and consider optimality criterion in reachability methods.

3. When RL Meets Feasible Sets

3.1. Notation

We formulate the CRL problem as an MDP with a deterministic dynamic (a reasonable assumption in safe control problems), defined by the tuple $\langle \mathcal{S}, \mathcal{A}, P, r, h, c, \gamma \rangle$ where (1) the state space \mathcal{S} and the action space \mathcal{A} are bounded (possibly continuous); (2) unknown transition probability $P : \mathcal{S} \times \mathcal{A} \times \mathcal{S} \mapsto \{0, 1\}$ represents the dynamic; (3) $r : \mathcal{S} \times \mathcal{A} \mapsto \mathbb{R}$ is the reward function; (4) $h : \mathcal{S} \mapsto \mathbb{R}$ is the state constraint. c is called the cost signal where $c(s) = \mathbb{1}_{h(s) > 0}$, indicating we get 1 if $h(s) \leq 0$ is violated and otherwise 0. (5) $\gamma \in (0, 1)$ is the discounted factor. A deterministic policy $\pi : \mathcal{S} \mapsto \mathcal{A}$ chooses action a_t at state

s_t at time t . The initial state distribution is denoted as $d_0(s)$ while $d_\pi(s, a)$ is the state-action marginals following π .

The objective of standard RL is to find a policy maximizing the expected return (discounted cumulative rewards) $\mathcal{J}(\pi) = \mathbb{E}_{s_t, a_t \sim d_\pi} \sum_t [\gamma^t r(s_t, a_t)]$. A value function $V^\pi(s) \triangleq \mathbb{E}_{s_t, a_t \sim d_\pi} \sum_t [\gamma^t r(s_t, a_t) | s_0 = s]$ represents the potential return in the future from state s , satisfying $V^\pi(s) = r(s, \pi(s)) + \gamma \mathbb{E}_{s' \sim P}[V^\pi(s')]$. One can easily find that $\mathcal{J}(\pi) = \mathbb{E}_{s \sim d_0(s)}[V^\pi(s)]$.

We need a few extended notations beyond standard ones. We denote $(s_t^\pi | s_0 = s, \pi), t \in \mathbb{N}$ as the state trajectory $\{s_0^\pi, s_1^\pi, \dots | s_0 = s, \pi\}$ induced by π from $s_0 = s$. Let $h(s_t^\pi | s_0 = s), t \in \mathbb{N}$ specify the state constraint sequence of the trajectory $\{h(s_0^\pi), h(s_1^\pi), h(s_2^\pi), \dots | s_0 = s, \pi\}$. We also denote $h(s_t^\pi | s_0 = s) \leq 0, t \in \mathbb{N}$ as persistently satisfying the constraint, i.e. $h(s_t^\pi) \leq 0, \forall t \in \mathbb{N}$.

3.2. Definition of Feasible Sets

Generally speaking, a state is considered *safe* if it satisfies the state constraint $h(s) \leq 0$, such as keeping distance from obstacles. The safe set is defined by the set of all safe states:

Definition 3.1 (Safe set).

$$\mathcal{S}_c \triangleq \{s | h(s) \leq 0\}.$$

However, as stated in Section 1, some safe states would go dangerous no matter what policy we choose, such as a high-speed vehicle close to an front obstacle. Therefore, what really matters for meaningful safety guarantee is not the *temporary* safety but the *persistent* safety, i.e., $h(s_t^\pi | s_0 = s) \leq 0, t \in \mathbb{N}$. Otherwise, the system will be dangerous sooner or later. In other words, we need to characterize those states starting from which the policy π is able to keep the system constraint-satisfactory. We define the feasible set as the set of all the states which are able to be safe persistently.

Definition 3.2 (Feasible set). The feasible set of a *specific* policy π can be defined as

$$\mathcal{S}_f^\pi \triangleq \{s \in \mathcal{S} | h(s_t^\pi | s_0 = s) \leq 0, t \in \mathbb{N}\}.$$

A policy π is feasible if $\mathcal{S}_f^\pi \neq \emptyset$ and otherwise it is infeasible. The largest feasible set \mathcal{S}_f is a subset of \mathcal{S} composed of states from which there exists *at least one* policy that keeps the system satisfying the constraint, i.e.,

$$\mathcal{S}_f \triangleq \{s \in \mathcal{S} | \exists \pi, h(s_t^\pi | s_0 = s) \leq 0, t \in \mathbb{N}\}.$$

To guarantee that all the states in the trajectory $\{s_t^\pi | s_0 = s, \pi\}, t \in \mathbb{N}$ are safe, we only need to guarantee that the worst-case i.e., the *maximum* violation in the trajectory is below zero, which brings the following definition:

Definition 3.3 (Safety value function).

$$V_h^\pi(s) \triangleq \max_{t \in \mathbb{N}} h(s_t^\pi | s_0 = s), \quad (1)$$

which is the worst constraint violation in the long term.

The safety value of a given state s varies when the policy π changes. The best value we can get is the one where we choose the policy minimizing the constraint violation and we call it the optimal safety value function:

$$V_h^*(s) \triangleq \min_{\pi} \max_{t \in \mathbb{N}} h(s_t^\pi | s_0 = s).$$

One can easily observe that the (largest) feasible set is the sub-zero level set of the (optimal) safety value function, i.e.,

$$\mathcal{S}_f^\pi = \{s | V_h^\pi(s) \leq 0\}, \quad \mathcal{S}_f = \{s | V_h^*(s) \leq 0\}.$$

and clearly $\mathcal{S}_f^\pi \subseteq \mathcal{S}_f$ for $\forall \pi$.

Unlike the common cost value function (i.e., discounted cumulative costs) in conventional CRL, the safety value function cares about the most dangerous state and measures the persistent safety of states. Safety problems in reality are more about the worst-case through time other than the cumulative or average costs (Fisac et al., 2019), where the latter is often the case in previous CRL. Specifically, if $V_h^*(s) \leq 0$, the safety of the system can be guaranteed by following the safest policy because the constraint is always satisfied. Otherwise, a state cannot be guaranteed safe and must be avoided. To conclude, the largest feasible set is what we need to specify the persistently safe states.

3.3. Computation of Feasible Sets

Although the safety value function does not use the discounted cumulative formulation like the common value functions in RL, we can still use the temporal difference learning technique to get it. Fisac et al. (2019) proposes the following lemma about the optimal safety value function:

Lemma 3.4 (Safety Bellman equation (SBE)).

$$V_h^*(s) = \max \left\{ h(s), \min_{a \in \mathcal{A}} V_h^*(s') \right\} \quad (2)$$

holds for $\forall s \in \mathcal{S}$, where s' is the successive state of state s .

We extend Lemma 3.4 to a general form applicable to any policy, which is called the self-consistency condition:

Theorem 3.5 (Self-consistency condition of the safety value function).

$$V_h^\pi(s) = \max \{ h(s), V_h^\pi(s') \} \quad (3)$$

holds for $\forall s \in \mathcal{S}$ and $\forall \pi$, where s' is the successive state at state s following π .

Proof. See Appendix B.1. \square

Remark 3.6. Obviously, the largest feasible set can be obtained by solving SBE (2) for the optimal safety value function. However, this will lead to a policy always pursuing the lowest constraint violation, i.e., a safety-oriented policy. Besides safety, other specifications do matter such as the performance optimality in RL. For example, a robotic arm should catch the objects as *quickly* as possible with only *bounded* torques. Intuitively, the safest action has to be taken only at states on the boundary of the feasible set (safety-critical states). We are free to choose different actions at the states which are interior points of the feasible set (non-safety-critical) (Asayesh et al., 2021). Therefore, if we optimize the expected return at non-safety-critical states and guarantee safety at safety-critical states, we are able to consider RL performance and safety comprehensively, where Theorem 3.5 will help.

4. Reachability Constrained Reinforcement Learning

In this section, we integrate the self-consistency condition (3) into the CRL framework and formally propose the problem statement of RCRL, followed by its benefits over conventional CMDP-based CRL methods and HJ reachability analysis methods. The feasible set of the solution to RCRL problem is equivalent to the largest one defined in Definition 3.2. A general RCRL algorithm with convergence guarantee will be devised.

4.1. Integrate Self-Consistency Condition to CRL

Previous CRL methods update cost value function in a bootstrap manner similar to value function in standard RL. However, states satisfying the cost value constraint $V_c^\pi(s) \leq \eta$ cannot guarantee persistent safety because this kind of constraint lacks physical interpretation. Furthermore, how to choose the threshold η is engineering-intuitive and task-specific. With the self-consistency condition of the safety value function, we can compute it with a bootstrap update as well. Thus, it is possible to replace the cost value constraint with constraints on the safety value function. It will not bother to design the threshold for safety value function because the feasible set is the sub-zero level set of the safety value function, so it is natural to choose zero. Therefore, it is more reasonable to choose $V_h^\pi(s) \leq 0$ to be the constraint in CRL and we call this inequality *reachability constraint*.

4.2. Problem Statement

Given an MDP defined in Section 3.1, RCRL aims to find an optimal policy π^* while fulfilling the reachability constraints:

$$\begin{aligned} \max_{\pi} \quad & \mathbb{E}_{s \sim d_0(s)}[V^\pi(s)] \\ \text{subject to} \quad & V_h^\pi(s) \leq 0, \forall s \in \mathcal{S}_f, \end{aligned} \quad (4)$$

where $\mathbb{E}_{s \sim d_0(s)}[V^\pi(s)]$ is the expected return, $V_h^\pi(s)$ is the safe value function of policy π , and the constraints require that π must guarantee the system safety starting from states inside the largest feasible set \mathcal{S}_f and act optimally.

Remark 4.1. One may question how we can get states from the largest feasible set before knowing it. We will explain it is reasonable from two aspects: (1) This setting is for the feasibility of problem (4) because if we impose constraints on states outside \mathcal{S}_f , there will be no solution. (2) Actually we sample states from a subspace $\mathcal{S}_{\text{sample}}$ of \mathcal{S} satisfying $\mathcal{S}_f \subseteq \mathcal{S}_{\text{sample}}$ so there must exist states outside \mathcal{S}_f . We will leverage the Lagrange multiplier method to solve it and according to complementary slackness condition (Bertsekas, 2016), the corresponding multipliers go to ∞ . However, we can set a sufficiently large bound for the multiplier to form a surrogate Lagrangian, preventing the divergence of Lagrangian. These states will not affect the policy optimization on feasible states because their corresponding multipliers are fixed after reaching the upper bound. Therefore, it is reasonable to impose constraints on states across the largest feasible set.

RCRL problem formulation has two significant advantages: (1) Compared to HJ reachability analysis studies, RCRL considers performance optimality criteria. (2) Compared to other RL methods with feasible sets, we guarantee that any feasible policy of RCRL renders the largest feasible sets, which brings less conservativeness and better performance. The second advantage is stated by the following proposition:

Proposition 4.2 (The largest feasible set). *Assuming $\mathcal{S}_f \neq \emptyset$, for any feasible π of problem (4), we have $\mathcal{S}_f^\pi = \mathcal{S}_f$.*

Proof. See Appendix B.2. \square

Proposition 4.2 reveals though the constraint in (4) is imposed on the safety value function of some policy, we can still capture the largest feasible set without computing the safest one, giving freedom to the policy in RCRL.

4.3. Lagrangian-Based Algorithm with Statewise Constraints

We leverage the Lagrangian-based methods to solve the RCRL problems, which is a common solution for CRL (Chow et al., 2017; Achiam & Amodei, 2019; Tessler et al., 2019). The key idea of Lagrangian-based methods is to descend in π and ascend in the Lagrange multiplier λ using the gradients of the Lagrangian $\mathcal{L}(\pi, \lambda)$ w.r.t. π and λ , respectively. Notably, that constraint in (4) is imposed on *each state* in \mathcal{S}_f , which is significantly different from typical constraints on only the expectation of the states in (Achiam et al., 2017; Chow et al., 2017; Tessler et al., 2019). We call these type of safety constraints as the *statewise constraints*. In these cases, the multiplier is not longer a scalar

but a infinite-dimension vector in infinite states cases. Some preliminary studies discuss statewise constraints only on the distribution density constraints (Chen & Ames, 2019; Qin et al., 2021). A more general Lagrangian-based solution for statewise constraints with *multiplier network* is discussed recently (Ma et al., 2021b;c). Without loss of generality, we denote the statewise multiplier as a function $\lambda : \mathcal{S} \mapsto [0, +\infty) \cup \{+\infty\}$. The Lagrangian of (4) can be formulated according to Theorem 7 in (Ma et al., 2021b):

$$\mathcal{L}(\pi, \lambda) = \mathbb{E}_{s \in \mathcal{S}_f} [-V^\pi(s) + \lambda(s)V_h^\pi(s)]. \quad (5)$$

Hence, the RCRL problem turns into finding the saddle point of (5):

$$\max_{\lambda} \min_{\pi} \mathcal{L}(\pi, \lambda). \quad (6)$$

Consider the common actor-critic framework with state-action value functions. We have the state-action (safety) value $Q(s, \pi(s)) = V^\pi(s)$ and $Q_h(s, \pi(s)) = V_h^\pi(s)$ due to the deterministic dynamic and policy. We also have parameterized Q-function $Q(s, a; \omega)$, safety Q-value function $Q_h(s, a; \phi)$, a policy $\pi(s; \theta)$, and the statewise multiplier $\lambda(s; \xi)$. The Lagrangian thus becomes $\mathcal{L}(\theta, \xi)$. Note that sometimes we use $Q_\omega, \pi_\theta, \lambda_\xi$ for short. Now we derive the objectives of the parameterized functions.

The Q-value function update is the standard one in popular RL (Sutton & Barto, 2018), which can be seen in Appendix A. The safety Q-value function of the current policy is updated according to respective self-consistency conditions in Lemma 3.4, i.e., minimizing the mean squared error:

$$\mathcal{J}_{Q_h}(\phi) = \mathbb{E}_{s \sim \mathcal{D}} \left[1/2 \left(Q_h(s, a; \phi) - \hat{Q}_h(s, a) \right)^2 \right], \quad (7)$$

where

$$\begin{aligned} \hat{Q}_h(s, a) &= (1 - \gamma)h(s) \\ &+ \gamma \mathbb{E}_{s' \sim P} [\max\{h(s), Q_h(s', \pi(s'); \phi)\}], \end{aligned} \quad (8)$$

\mathcal{D} is a distribution over states across the largest feasible set according to Remark 4.1, and a is the action taken at s . Note that the discounted version of self-consistency condition is for convergence in Appendix B.3 (Fisac et al., 2019).

As aforementioned, the purpose of policy π_θ is to descend the Lagrangian while the multiplier tries to ascend it:

$$\begin{aligned} \mathcal{J}_\pi(\theta) &= \mathcal{J}_\lambda(\xi) \\ &= \mathbb{E}_{s \sim \mathcal{D}} [-Q(s, \pi_\theta(s); \omega) + \lambda_\xi(s)Q_h(s, \pi_\theta(s); \phi)]. \end{aligned} \quad (9)$$

Algorithm 1 provides the pseudo-code of an actor-critic version of RCRL. The algorithm alternates between interacting with the environment and updating the parameter vectors with stochastic gradients $\hat{\nabla}_\omega \mathcal{J}_Q(\omega)$, $\hat{\nabla}_\theta \mathcal{J}_\pi(\theta)$,

Algorithm 1 Template for actor-critic RCRL

Input: MDP M with constraint $h(\cdot)$, critic and safety value function learning rate $\beta_1(k)$, actor learning rate $\beta_2(k)$, multiplier learning rate $\beta_3(k)$

Initialization: q-function parameters $\omega = \omega_0$, safety q-function parameters $\phi = \phi_0$, policy parameters $\theta = \theta_0$, multiplier parameters $\xi = \xi_0$

for $k = 0, 1, \dots$ **do**

 Initialize state $s_0 \sim d_0$.

for $t = 0$ **to** $T - 1$ **do**

 Select action $a_t = \pi_\theta(s_t)$, observe next state s_{t+1} , reward r_t and constraint $h(s_t)$

Critic update $\omega_{k+1} = \omega_k - \beta_1(k) \hat{\nabla}_\omega \mathcal{J}_Q(\omega)$

Safety value update

$$\phi_{k+1} = \phi_k - \beta_1(k) \hat{\nabla}_\phi \mathcal{J}_{Q_h}(\phi)$$

Actor update $\theta_{k+1} = \Gamma_\Theta \left(\theta_k - \beta_2(k) \hat{\nabla}_\theta \mathcal{J}_\pi(\theta) \right)$

Multiplier update

$$\xi_{k+1} = \Gamma_\Xi \left(\xi_k + \beta_3(k) \hat{\nabla}_\xi \mathcal{J}_\lambda(\xi) \right)$$

end for

end for

return parameters $\omega, \phi, \theta, \xi$

$\hat{\nabla}_\theta \mathcal{J}_\pi(\theta)$, and $\hat{\nabla}_\xi \mathcal{J}_\lambda(\xi)$, whose derivation can be seen in Appendix A. In the algorithm, the $\Gamma_\Psi(\psi)$ operator projects a vector $\psi \in \mathbb{R}^\kappa$ to the closet point in a compact and convex set $\Psi \subset \mathbb{R}^\kappa$, i.e., $\Gamma_\Psi(\psi) = \arg \min_{\hat{\psi} \in \Psi} \|\hat{\psi} - \psi\|^2$ where ψ is denoted as any one of θ, ξ . These projection operators are necessary for the convergence of the actor-critic algorithm (Chow et al., 2017). A policy-gradient version of RCRL is designed similarly in Algorithm 2.

5. Convergence Analysis

Under moderate assumptions, we can provide a convergence guarantee of Algorithm 1. The convergence analysis follows heavily from the convergence proof of multi-time scale stochastic approximation algorithms (Chow et al., 2017). We also utilize theorems of combining the ODE (ordinary differential equation) viewpoint and stochastic approximation from (Borkar, 2009). We first introduce the necessary assumptions.

Assumption 5.1 (Finite MDP). The MDP is finite (finite state and action space, i.e., $|\mathcal{S}| < \infty, |\mathcal{A}| < \infty$), and \mathcal{S} and \mathcal{A} are both bounded. The first-hitting time of the MDP $T_{\pi, s}$ is bounded almost surely over all policy π and all initial states $s \in \mathcal{S}$. We refer the upper bound as T . The reward function of a single step is bounded by r_{\max} . Hence, the value function is upper bounded by $r_{\max}/(1 - \gamma)$.

Assumption 5.2 (Strict Feasibility). There exists a policy $\pi(\cdot; \theta)$ such that $V_h^{\pi_\theta}(s) \leq 0, \forall s \in \mathcal{S}_f$.

Assumption 5.3 (Differentiability). For any state-action

pair (s, a) , $Q(s, a; \omega)$ and $Q_h(s, a; \phi)$ are continuously differentiable in ω and ϕ , respectively. Moreover, $\nabla_a Q(s, a; \omega)$ and $\nabla_a Q_h(s, a; \phi)$ are Lipschitz functions in a , for $\forall s \in \mathcal{S}, \forall \omega \in \Omega$, and $\forall \phi \in \Phi$. For $\forall s \in \mathcal{S}, \forall a \in \mathcal{A}$, $\nabla_a Q(s, a; \omega)$ is a Lipschitz function in ω and $\nabla_a Q_h(s, a; \phi)$ is a Lipschitz function in ϕ . For any state s , $\pi(s; \theta)$ is continuously differentiable in θ and $\nabla_\theta \pi(s; \theta)$ is a Lipschitz function in θ . For any state s , $\lambda(s; \xi)$ is continuously differentiable in ξ and $\nabla_\xi \lambda(s; \xi)$ is a Lipschitz function in ξ .

Assumption 5.4 (Step Sizes). The step size schedules $\{\beta_1(k)\}$, $\{\beta_2(k)\}$, and $\{\beta_3(k)\}$ satisfy

$$\begin{aligned} \sum_k \beta_1(k) &= \sum_k \beta_2(k) = \sum_k \beta_3(k) = \infty \\ \sum_k \beta_1(k)^2, \sum_k \beta_2(k)^2, \sum_k \beta_3(k)^2 &< \infty \\ \beta_3(k) &= o(\beta_2(k)), \beta_2(k) = o(\beta_1(k)). \end{aligned}$$

These step-size schedules satisfy the standard conditions for stochastic approximation algorithms, and ensure that the critic update is on the fastest time scale $\{\beta_1(k)\}$, the policy update is on the intermediate time scale $\{\beta_2(k)\}$, and the multiplier is on the slowest one $\{\beta_3(k)\}$. Now we come to the position where the convergence of actor-critic RCRL can be provided.

Theorem 5.5. *Under Assumption 5.1 to 5.4, the policy sequence updated in Algorithm 1 converges almost surely to a locally optimal policy for the reachability constrained policy optimization problem (4).*

Proof. See Appendix B.3. \square

The conditions for convergence may be strict and ideal such that we have to make some simplification and approximation to make the RCRL algorithm tractable and scalable for high-dimensional and continuous problems. We will discuss the gap between the necessary assumptions and the practical situation in Appendix C.1. More details about implementation can be found in Appendix C.

6. Experiments

We aim to answer the following through our experiments:

- Can RCRL learn the largest feasible sets using neural networks approximation of safety value functions?
- Does RCRL outperform CRL methods based on cost value constraints with fewer violations?
- Does RCRL perform better than methods based on energy function with respect to performance optimality benefiting from the largest feasible set?

Benchmarks. We implement both on- and off-policy RCRL and compare them with different CRL baselines. Experiments include that: (1) use double-integrator (Fisac et al., 2019) which has an analytical solution to check the correctness of feasible set learned by RCRL; (2) validate the scalability of RCRL to nonlinear control problems, specifically, a 2D quadrotor trajectory tracking task in safe-control-gym (Yuan et al., 2021), and (3) classical safe learning benchmark Safety-Gym (Achiam & Amodei, 2019). Details about each benchmark will be introduced per subsection.

Baseline Algorithms. Details about algorithms can be seen in Appendix C. Besides RCRL, we test following baselines: (1) **Lagrangian**-based algorithms whose constraint is about the discounted cumulative costs (similar with RCPO (Tessler et al., 2019)); (2) **Reward shaping** method with a fixed coefficient penalty added to the reward; (3) **CBF**-based algorithms whose constraint is about $B(s) \triangleq \dot{h}(s) + \mu h(s) \leq 0$ where $\mu \in (0, 1)$ is a hyperparameter; and (4) **SI**-based methods that defines an SI $\varphi(s) = \sigma - (-h(s))^n + k\dot{h}(s)$ and sets constraints

$$\varphi(s') - \max\{\varphi(s) - \eta_D, 0\} \leq 0, \quad (10)$$

where σ, n, k, η_D are hyperparameters.

6.1. Double Integrator: Comparison to Ground Truth

We demonstrate that RCRL can learn the largest feasible sets when controlling the double integrator. The reason why we choose the double integrator is that it is a simple dynamical system where we can use numerical solution by the level set toolbox to obtain the ground truth about the largest feasible sets (also called *HJ viability kernels*) (Mitchell, 2008). Double integrator is a 2D dynamical system, where the system states and the dynamics are denoted as

$$s = [x_1, x_2]^T, \quad \dot{s} = [x_2, a], \quad (11)$$

where the control limits of action a is $a \in [-0.5, 0.5]$. The safety constraint is $\|s\|_\infty \leq 5$. The reward is designed as $r_t = \|s\|^2 + a_t^2$.

Baselines. In addition to the ground truth using the level set toolbox (Mitchell, 2008), we introduce two discrete approximations of feasible sets using model predictive control (MPC) utilizing CBF constraints and terminal constraints, respectively (Ma et al., 2021a; Mayne et al., 2000). These two MPC baselines are named as MPC-CBF and MPC-Terminal, respectively.

The learned result is shown in Figure 2. It depicts that the learned \mathcal{S}_f^T exactly approximate the largest feasible set or the HJ viability kernel which is numerically computed by the level set toolbox. MPC-Terminal also identifies the feasible sets with some discretization error. MPC-CBF has a smaller feasible set since the conservativeness of energy-based methods.

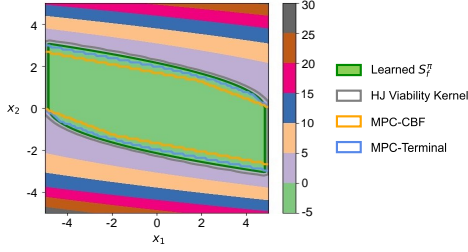


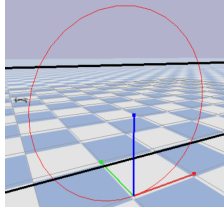
Figure 2. Learned S_f^π of the double integrator.

6.2. Safe-control-gym: Quadrotor Trajectory Tracking

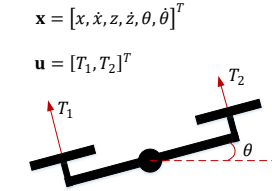
The 2D quadrotor trajectory tracking task comes from safe-control-gym (Yuan et al., 2021) and is shown in Figure 3(a), where the circle trajectory is marked as red and the constraint for the quadrotor is to keep itself between the two black lines. Schematics of the 2D quadrotor are shown in Figure 3(b), where (x, z) and (\dot{x}, \dot{z}) are the position and velocity of the COM (center of mass) of the quadrotor in the xz -plane, and θ and $\dot{\theta}$ are the pitch angle and pitch angle rate, respectively. The task for the quadrotor is to track the moving waypoint on the circle trajectory by controlling the normalized thrusts while maintaining its altitude z between $[0.5, 1.5]$, i.e.,

$$h(s) = \max\{0.5 - s^{(2)}, s^{(2)} - 1.5\}.$$

Details about the state and action space, reward function can be seen in Appendix D.1.



(a) Snapshot of environment, where red line is the reference and black lines are constraint boundaries.



(b) Schematics, state and input of the 2D quadrotor

Figure 3. safe-control-gym environment

Baselines. We implement an off-policy version of RCRL in safe-control-gym based on SAC (Haarnoja et al., 2018), forming our Reachable Actor Critic (RAC). Other off-policy baselines are all implemented based on SAC for fairness, including: (1) **SAC-Lagrangian**, (2) **SAC-Reward Shaping**, (3) **SAC-CBF**, and (4) **SAC-SI**.

Figure 4 demonstrates performance with respect to the average return and constraint violation rate of the five algorithms. RAC (blue line) learns a zero-violation policy and reaches

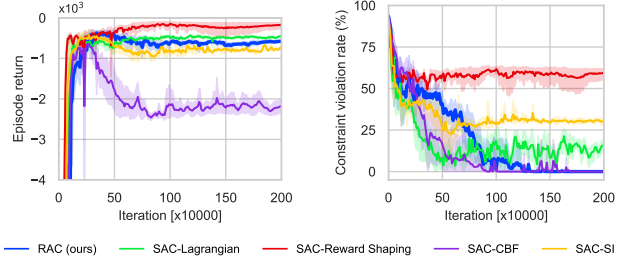


Figure 4. Performance of algorithms on safety-control-gym. The first two figures are training curves on the quadrotor trajectory tracking task. All results are averaged on 5 independent runs and the shaded regions are the 95% confidence intervals.

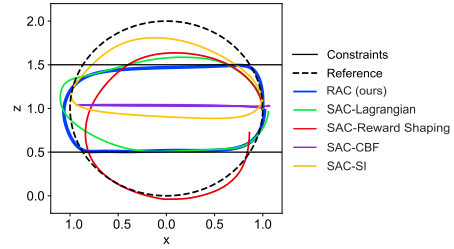


Figure 5. Trajectories of final policies trained by different algorithms in a run.

near-optimal tracking accuracy. In contrast, though SAC-CBF does not violate the constraint as well, the tracking error is quite large because it just moves horizontally due to a conservative policy. The constraints of SAC-SI require the SI to be below zero and to decrease when it is beyond zero, which explains that it makes the quadrotor fly beyond the upper bound and move horizontally in the safe set, corresponding to the feasible set in Figure 6(c). The other two algorithms reach higher returns at the cost of unacceptable constraint violation. In this task, keeping z between $[0.5, 1.5]$ will definitely bring tracking error, which leads to a lower return. Trajectories in Figure 5 indicate that RAC keeps the quadrotor in the safe set strictly and tracks the trajectory accurately inside the safe set while others fail to.

Figure 6 shows the slices on xz -plane of the feasible sets learned by RAC, SAC-CBF, and SAC-SI with $\dot{z} = -1, 0, 1$. The sub-zero level set of each constrained function represents the learned feasible sets, i.e. $\{s \mid F^\pi(s, a; \phi) \leq 0\}$ where $F = Q_h, B$, or φ . In Figure 6(a), the feasible sets of RAC (inside the zero-contour) is smaller than S_c because when the quadrotor at the boundary of S_c with a velocity pointing outside, it is doomed to fly out of the space, leading to constraint violation. Thus, such states are supposed to be potentially dangerous and must have a super-zero safety value. Characterizing the feasible set helps RAC track the trajectory accurately inside the safe set (*optimality*) and satisfy the constraint strictly (*safety*). In contrast, an energy function like CBF or SI relies on prior knowledge about the

dynamical system. When we choose empirical hyperparameters, the algorithms will possibly learn the wrong feasible set, which leads to either constraint violation or poor performance. As shown in Figure 6(b) and 6(c), when $\dot{z} \neq 0$, the whole safe set is considered unsafe because of conservativeness. SAC-CBF considers $\dot{z} = 0$ as safe, leading to a horizontal-moving policy while SAC-SI leans a wrong feasible set when $\dot{z} = 0$, leading to its poor performance.

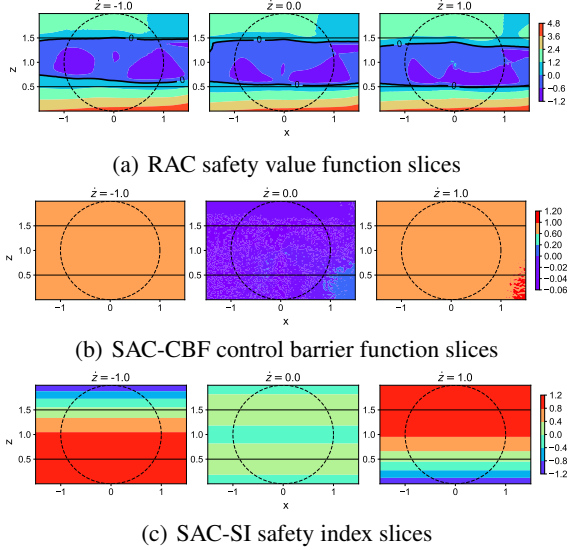


Figure 6. The learned feasible set slices on the 2D xz -plane with different \dot{z} . Values below zero mean feasibility.

6.3. Safety-Gym: Moving with Sensor Inputs

All previous tasks have full knowledge of the exact system states in the observations. In this section, we demonstrate the effectiveness of RCRL in complex safe control tasks with only high-dimensional sensor inputs, such as Lidar. In these tasks, the agent must achieve the goal position without stepping into dangerous hazards or colliding with the pillars, demonstrated in Figure 7.

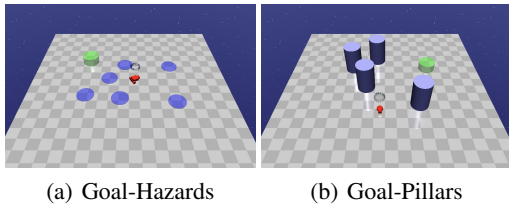


Figure 7. Safety-Gym tasks.

Baselines. We name the *on-policy* version of RCRL as Reachability Constrained Optimization (**RCO**). Baseline algorithms in Safety-Gym tasks include traditional CRL baseline **PPO-Lagrangian** (Schulman et al., 2017; Achiam & Amodei, 2019) and two constrained version of PPO with energy-function based constraints (named as **PPO-CBF** and

PPO-SI), and unconstrained baseline **PPO**. The distance and relative speed are approximated from the Lidar and speedometer sensors. For multiple obstacles, we select the one with the closest distance (in RCO) or the highest safety energy (in PPO-SI and PPO-CBF) to compute the safety value functions or energy functions used for constraints.

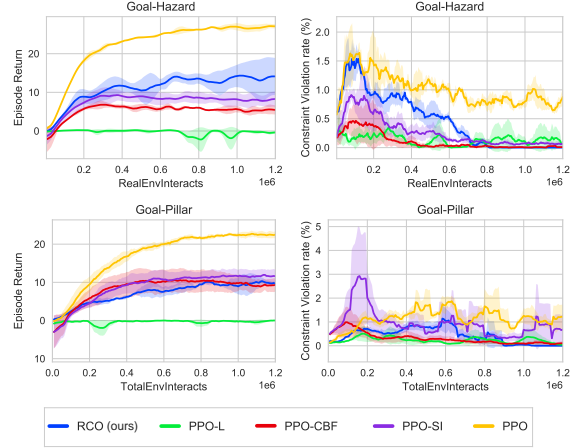


Figure 8. Training results of Safety-Gym tasks.

The training results are shown in Figure 8. The violation rate figures indicate that RCO has the best constraint satisfaction performance, while energy-based baselines PPO-CBF, PPO-SI oscillate around zero violation, indicating RCO learns the feasible sets more exactly. On the contrary, the prior parameters of SI and CBF fail to characterize the exact feasible sets. Meanwhile, RCO has comparable or better return performance, further verifying that RCO reduces the conservativeness compared to energy-based methods.

7. Conclusion and Future Works

We study a novel reachability constraint in CRL, where the safety value function is constrained, guaranteeing persistent constraint-satisfaction. We establish the self-consistency condition of the safety value function, which enables us to characterize the largest feasible set in CRL and consider performance optimality besides safety, avoiding the safety-oriented policies in prior HJ reachability analysis methods. We also prove the convergence of the proposed RCRL with multi-time scale stochastic approximation theory under mild assumptions. However, there is still constraint-violation during the early stage of training of RCRL agents. We will try to improve RCRL with different approaches such as model-based methods for safe exploration and safe learning in the future.

References

Achiam, J. and Amodei, D. Benchmarking safe exploration in deep reinforcement learning. 2019.

- Achiam, J., Held, D., Tamar, A., and Abbeel, P. Constrained policy optimization. In *International Conference on Machine Learning*, pp. 22–31. PMLR, 2017.
- Altman, E. *Constrained Markov decision processes*, volume 7. CRC Press, 1999.
- Ames, A. D., Coogan, S., Egerstedt, M., Notomista, G., Sreenath, K., and Tabuada, P. Control barrier functions: Theory and applications. In *2019 18th European Control Conference (ECC)*, pp. 3420–3431. IEEE, 2019.
- Asayesh, S., Chen, M., Mehrandezh, M., and Gupta, K. Toward observation based least restrictive collision avoidance using deep meta reinforcement learning. *IEEE Robotics and Automation Letters*, 6(4):7445–7452, 2021. doi: 10.1109/LRA.2021.3098332.
- Bansal, S. and Tomlin, C. J. Deepreach: A deep learning approach to high-dimensional reachability. In *2021 IEEE International Conference on Robotics and Automation (ICRA)*, pp. 1817–1824. IEEE, 2021.
- Bansal, S., Chen, M., Herbert, S., and Tomlin, C. J. Hamilton-jacobi reachability: A brief overview and recent advances. In *2017 IEEE 56th Annual Conference on Decision and Control (CDC)*, pp. 2242–2253. IEEE, 2017.
- Bertsekas, D. P. *Nonlinear programming*. Athena Scientific, 2016.
- Bharadhwaj, H., Kumar, A., Rhinehart, N., Levine, S., Shkurti, F., and Garg, A. Conservative safety critics for exploration. *arXiv preprint arXiv:2010.14497*, 2020.
- Borkar, V. S. *Stochastic approximation: a dynamical systems viewpoint*, volume 48. Springer, 2009.
- Brunke, L., Greeff, M., Hall, A. W., Yuan, Z., Zhou, S., Panerati, J., and Schoellig, A. P. Safe learning in robotics: From learning-based control to safe reinforcement learning, 2021.
- Chen, Y. and Ames, A. D. Duality between density function and value function with applications in constrained optimal control and markov decision process. *arXiv preprint arXiv:1902.09583*, 2019.
- Choi, J. J., Lee, D., Sreenath, K., Tomlin, C. J., and Herbert, S. L. Robust control barrier-value functions for safety-critical control. *arXiv preprint arXiv:2104.02808*, 2021.
- Chow, Y., Ghavamzadeh, M., Janson, L., and Pavone, M. Risk-constrained reinforcement learning with percentile risk criteria. *The Journal of Machine Learning Research*, 18(1):6070–6120, 2017.
- Dawson, C., Qin, Z., Gao, S., and Fan, C. Safe nonlinear control using robust neural lyapunov-barrier functions. *arXiv preprint arXiv:2109.06697*, 2021.
- Duan, J., Guan, Y., Li, S. E., Ren, Y., Sun, Q., and Cheng, B. Distributional soft actor-critic: Off-policy reinforcement learning for addressing value estimation errors. *IEEE Transactions on Neural Networks and Learning Systems*, pp. 1–15, 2021a. doi: 10.1109/TNNLS.2021.3082568.
- Duan, J., Liu, Z., Li, S. E., Sun, Q., Jia, Z., and Cheng, B. Adaptive dynamic programming for non-affine nonlinear optimal control problem with state constraints. *Neurocomputing*, 2021b. ISSN 0925-2312. doi: <https://doi.org/10.1016/j.neucom.2021.04.134>. URL <https://www.sciencedirect.com/science/article/pii/S0925231221015848>.
- Fisac, J. F., Lugovoy, N. F., Rubies-Royo, V., Ghosh, S., and Tomlin, C. J. Bridging hamilton-jacobi safety analysis and reinforcement learning. In *2019 International Conference on Robotics and Automation (ICRA)*, pp. 8550–8556, 2019. doi: 10.1109/ICRA.2019.8794107.
- Fujimoto, S., van Hoof, H., and Meger, D. Addressing function approximation error in actor-critic methods. In Dy, J. and Krause, A. (eds.), *Proceedings of the 35th International Conference on Machine Learning Research*, pp. 1587–1596. PMLR, 10–15 Jul 2018. URL <https://proceedings.mlr.press/v80/fujimoto18a.html>.
- Guan, Y., Duan, J., Li, S. E., Li, J., Chen, J., and Cheng, B. Mixed policy gradient. *arXiv preprint arXiv:2102.11513*, 2021a.
- Guan, Y., Ren, Y., Sun, Q., Li, S. E., Ma, H., Duan, J., Dai, Y., and Cheng, B. Integrated decision and control: Towards interpretable and computationally efficient driving intelligence. *arXiv preprint arXiv:2103.10290*, 2021b.
- Haarnoja, T., Zhou, A., Abbeel, P., and Levine, S. Soft actor-critic: Off-policy maximum entropy deep reinforcement learning with a stochastic actor. In Dy, J. and Krause, A. (eds.), *Proceedings of the 35th International Conference on Machine Learning Research*, pp. 1861–1870. PMLR, 10–15 Jul 2018. URL <https://proceedings.mlr.press/v80/haarnoja18b.html>.
- Hsu, K.-C., Rubies-Royo, V., Tomlin, C. J., and Fisac, J. F. Safety and liveness guarantees through reach-avoid reinforcement learning. *arXiv preprint arXiv:2112.12288*, 2021.
- Khalil, H. K. and Grizzle, J. *Nonlinear systems*. Prentice hall Upper Saddle River, 2002.

- Kim, H., Papamakarios, G., and Mnih, A. The lipschitz constant of self-attention. In Meila, M. and Zhang, T. (eds.), *Proceedings of the 38th International Conference on Machine Learning*, volume 139 of *Proceedings of Machine Learning Research*, pp. 5562–5571. PMLR, 18–24 Jul 2021. URL <https://proceedings.mlr.press/v139/kim21i.html>.
- Lillicrap, T. P., Hunt, J. J., Pritzel, A., Heess, N., Erez, T., Tassa, Y., Silver, D., and Wierstra, D. Continuous control with deep reinforcement learning. In *ICLR (Poster)*, 2016. URL <http://arxiv.org/abs/1509.02971>.
- Liu, C. and Tomizuka, M. Control in a safe set: Addressing safety in human-robot interactions. In *Dynamic Systems and Control Conference*, volume 46209, pp. V003T42A003. American Society of Mechanical Engineers, 2014.
- Lygeros, J., Tomlin, C., and Sastry, S. Controllers for reachability specifications for hybrid systems. *Automatica*, 35(3):349–370, 1999.
- Ma, H., Chen, J., Li, S., Lin, Z., Guan, Y., Ren, Y., and Zheng, S. Model-based constrained reinforcement learning using generalized control barrier function. In *2021 IEEE/RSJ International Conference on Intelligent Robots and Systems (IROS)*, pp. 4552–4559, 2021a. doi: 10.1109/IROS51168.2021.9636468.
- Ma, H., Guan, Y., Li, S. E., Zhang, X., Zheng, S., and Chen, J. Feasible actor-critic: Constrained reinforcement learning for ensuring statewise safety. *arXiv preprint arXiv:2105.10682*, 2021b.
- Ma, H., Liu, C., Li, S. E., Zheng, S., and Chen, J. Joint synthesis of safety certificate and safe control policy using constrained reinforcement learning. *arXiv preprint arXiv:2111.07695*, 2021c.
- Mayne, D. Q., Rawlings, J. B., Rao, C. V., and Sokaert, P. O. Constrained model predictive control: Stability and optimality. *Automatica*, 36(6):789–814, 2000.
- Mitchell, I. The flexible, extensible and efficient toolbox of level set methods. *Journal of Scientific Computing*, 35: 300–329, 2008. doi: 10.1007/s10915-007-9174-4.
- Mitchell, I., Bayen, A., and Tomlin, C. A time-dependent hamilton-jacobi formulation of reachable sets for continuous dynamic games. *IEEE Transactions on Automatic Control*, 50(7):947–957, 2005. doi: 10.1109/TAC.2005.851439.
- Qin, Z., Chen, Y., and Fan, C. Density constrained reinforcement learning. In Meila, M. and Zhang, T. (eds.), *Proceedings of the 38th International Conference on Machine Learning*, volume 139 of *Proceedings of Machine Learning Research*, pp. 8682–8692. PMLR, 18–24 Jul 2021. URL <https://proceedings.mlr.press/v139/qin21a.html>.
- Rockafellar, R. T. *Convex analysis*. Princeton university press, 2015.
- Schulman, J., Wolski, F., Dhariwal, P., Radford, A., and Klimov, O. Proximal policy optimization algorithms. *arXiv preprint arXiv:1707.06347*, 2017.
- Silver, D., Lever, G., Heess, N., Degris, T., Wierstra, D., and Riedmiller, M. Deterministic policy gradient algorithms. In *International conference on machine learning*, pp. 387–395. PMLR, 2014.
- Sutton, R. S. and Barto, A. G. *Reinforcement learning: An introduction*. MIT press, 2018.
- Tessler, C., Mankowitz, D. J., and Mannor, S. Reward constrained policy optimization. In *International Conference on Learning Representations*, 2019. URL <https://openreview.net/forum?id=SkfrvsA9FX>.
- Yang, T.-Y., Rosca, J., Narasimhan, K., and Ramadge, P. J. Projection-based constrained policy optimization. In *International Conference on Learning Representations*, 2020. URL <https://openreview.net/forum?id=rke3TJrtPS>.
- Yuan, Z., Hall, A. W., Zhou, S., Brunke, L., Greeff, M., Panerati, J., and Schoellig, A. P. safe-control-gym: a unified benchmark suite for safe learning-based control and reinforcement learning. *arXiv preprint arXiv:2109.06325*, 2021.
- Zhang, J., He, T., Sra, S., and Jadbabaie, A. Why gradient clipping accelerates training: A theoretical justification for adaptivity. In *International Conference on Learning Representations*, 2020. URL <https://openreview.net/forum?id=BJgnXpVYwS>.
- Zhao, W., He, T., and Liu, C. Model-free safe control for zero-violation reinforcement learning. In *5th Annual Conference on Robot Learning*, 2021. URL <https://openreview.net/forum?id=UGp6FDaxB0f>.

A. Loss Function and Gradients Derivation

The Q-value loss is the mean square error between the approximated Q function and its target (Lillicrap et al., 2016):

$$\mathcal{J}_Q(\omega) = \mathbb{E}_{s \sim \mathcal{D}}[1/2(Q(s, a; \omega) - \hat{Q}(s, a))^2] \quad (12)$$

where

$$\hat{Q}(s, a) = r(s, a) + \gamma \mathbb{E}_{s' \sim P}[Q(s', \pi(s'); \omega)].$$

Therefore, we are able to derive the stochastic gradients of each objective w.r.t. the parameter vectors in the approximate function. A sample (s_t, a_t, s_{t+1}) at time step t is leveraged to compute the stochastic gradients. First, (12) and (7) can be optimized with stochastic gradients descent (SGD):

$$\begin{aligned} \hat{\nabla}_{\omega} \mathcal{J}_Q(\omega) &= \nabla_{\omega} Q(s_t, a_t; \omega) \cdot (Q_{\omega}(s_t, a_t) - (r(s_t, a_t) + \gamma Q(s_{t+1}, a_{t+1}; \omega))), \\ \hat{\nabla}_{\phi} \mathcal{J}_{Q_h}(\phi) &= \nabla_{\phi} Q_h(s_t, a_t; \phi) \cdot (Q_h(s_t, a_t; \phi) - (h(s) + \gamma Q_h(s_{t+1}, a_{t+1}; \phi))), \end{aligned} \quad (13)$$

where $a_{t+1} = \pi(s_{t+1})$.

Combining results from (Silver et al., 2014; Lillicrap et al., 2016), the estimated deterministic policy gradient (DPG) is

$$\hat{\nabla}_{\theta} \mathcal{J}_{\pi}(\theta) = \nabla_a (-Q_{\omega}(s_t, a_t) + \lambda_{\xi}(s_t) Q_h(s_t, a_t; \phi))|_{a=a_t} \cdot \nabla_{\theta} \pi_{\theta}(s_t). \quad (14)$$

Then the stochastic gradient of the multiplier is used to ascend (9):

$$\hat{\nabla}_{\xi} \mathcal{J}_{\lambda}(\xi) = Q_h(s_t, \pi_{\theta}(s_t); \phi) \nabla_{\xi} \lambda_{\xi}(s_t). \quad (15)$$

B. Proofs

B.1. Proof of Equation (2)

We only prove the self-consistency condition because the safety Bellman equation can be proven similarly. From the definition of the safety value function, we know that

$$\begin{aligned} V_h^{\pi}(s) &= \max_{t \in \mathbb{N}} h(s_t^{\pi} \mid s_0 = s) \\ &= \max\{h(s), \max_{t \in \mathbb{N}^+} h(s_t^{\pi} \mid s_0 = s)\} \\ &= \max\{h(s), \max_{t \in \mathbb{N}^+} h(s_t^{\pi} \mid s_1 = s')\} \\ &= \max\{h(s), \max_{t \in \mathbb{N}} h(s_t^{\pi} \mid s_0 = s')\} \\ &= \max\{h(s), V_h^{\pi}(s')\}, \end{aligned} \quad (16)$$

where $s' \sim P(\cdot \mid s, \pi(s))$.

B.2. Proof of Proposition 4.2

It is obvious that $\mathcal{S}_f^{\pi} \subseteq \mathcal{S}_f$, we only need to prove that $\mathcal{S}_f \subseteq \mathcal{S}_f^{\pi}$. For any $s \in \mathcal{S}_f$, according to the constraint in (4), we have $V_h^{\pi}(s) \leq 0$, thus we have $s \in \mathcal{S}_f^{\pi}$ by Definition 3.2. Therefore, $\mathcal{S}_f \subseteq \mathcal{S}_f^{\pi}$.

B.3. Proof of Theorem 5.5

The proof borrows heavily from (Chow et al., 2017) and (Ma et al., 2021c) which both follow the convergence proof of multi-time scale stochastic approximation algorithms in (Borkar, 2009). A high level overview of the proof structure is shown as follows.

1. By utilizing policy evaluation techniques, we show the critic and safety value function update converge (in the fastest time scale) almost surely to a fixed point solution (ω^*, ϕ^*) .

2. Then, by convergence properties of multi-time scale discrete stochastic approximation algorithms, we show that each update (θ_k, ξ_k) converges almost surely to a stationary point (θ^*, ξ^*) of the corresponding continuous time system but with different speeds.
3. By using Lyapunov analysis, we show that the continuous time system is locally asymptotically stable at the stationary point (θ^*, ξ^*) .
4. Since the Lyapunov function used in the above analysis is the Lagrangian function $\mathcal{L}(\theta, \xi)$, we conclude that the stationary point (θ^*, ξ^*) is a local saddle point. Finally by the local saddle point theorem, we deduce that θ^* is a locally optimal solution for the reachability constrained RL problem.

Time scale 1 (Convergence of ω - and ϕ -updates) The step size assumption tells that $\{\omega_k\}$ and $\{\phi_k\}$ converges on a faster time scale than $\{\theta_k\}$ and $\{\xi_k\}$. According to (Borkar, 2009, Lemma 1, Chapter 6), we can treat (θ, ξ) as arbitrarily fixed quantities during updating $\{\omega_k\}$ and $\{\phi_k\}$. Therefore, we take $(\theta, \xi) = (\theta_k, \xi_k)$, which means the policy and the multiplier are fixed and we are performing policy evaluation to compute $Q^\pi(s, a)$ and $Q_h^\pi(s, a)$. With the standard policy evaluation convergence results in (Sutton & Barto, 2018), one can easily know that $Q(s, a; \omega_k) \rightarrow Q(s, a; \omega^*) = Q^{\pi_{\theta_k}}(s, a)$ as $k \rightarrow \infty$ because the operator \mathcal{B} defined by

$$\mathcal{B}[Q(s, a)] = r(s, a) + \gamma \mathbb{E}_{s' \sim P}[Q(s', \pi(s'))]$$

is a γ contraction mapping. Thus, all we need to do is to prove that the safety value evaluation in (8) is a γ -contraction mapping as well, which is stated in the following Lemma.

Lemma B.1 (γ -contraction Mapping). *Under Assumption 5.1, the operator \mathcal{B}_h introduced by $\mathcal{B}_h[Q_h(s, a)] = (1 - \gamma)h(s) + \gamma \max\{h(s), \mathbb{E}_{s' \sim P}[Q_h(s', \pi(s'))]\}$ is a γ -contraction mapping.*

Proof. We study the supremum norm of \mathcal{B}_h . For any Q_h and \hat{Q}_h , the following holds:

$$\begin{aligned} \|\mathcal{B}_h[Q_h(s, a)] - \mathcal{B}_h[\hat{Q}_h(s, a)]\|_\infty &= \gamma \|\max\{h(s), \mathbb{E}_{s' \sim P}[Q_h(s', \pi(s'))]\} - \max\{h(s), \mathbb{E}_{s' \sim P}[\hat{Q}_h(s', \pi(s'))]\}\|_\infty \\ &\leq \gamma \|\mathbb{E}_{s' \sim P}[Q_h(s', \pi(s'))] - \mathbb{E}_{s' \sim P}[\hat{Q}_h(s', \pi(s'))]\|_\infty \\ &= \gamma \|\mathbb{E}_{s' \sim P}[Q_h(s', \pi(s')) - \hat{Q}_h(s', \pi(s'))]\|_\infty \\ &\leq \gamma \|Q_h(s, a) - \hat{Q}_h(s, a)\|_\infty. \end{aligned}$$

□

According to (Bertsekas, 2016, Proposition A.26), we can conclude that $Q_h(s, a; \phi)$ will converge to $Q_h(s, a; \phi^*) = Q_h^{\pi_{\theta_k}}(s, a)$ as $k \rightarrow \infty$. Hence, both ω_k and ϕ_k converge to ω^* and ϕ^* , respectively and the convergence of **Time scale 1** is proved.

Time scale 2 (Convergence of θ -update) Due to the faster convergence speed than ξ_k , we can take $\xi = \xi_k$ when updating θ according to (Borkar, 2009, Lemma. 1, Chapter 6). Furthermore, since ω and ϕ converge on a faster speed than θ , we have $\|Q(s, a; \omega_k) - Q^{\pi_{\theta_k}}(s, a)\| \rightarrow 0$ and $\|Q_h(s, a; \phi_k) - Q_h^{\pi_{\theta_k}}(s, a)\| \rightarrow 0$ almost surely. Assume that the sample distribution is the same as \mathcal{D} . The θ -update from (14) is

$$\theta_{k+1} = \Gamma_\Theta [\theta_k - \beta_2(k) \nabla_a (-Q_{\omega_k}(s_t, a_t) + \lambda_\xi(s_t) Q_h(s_t, a_t; \phi_k)) \cdot \nabla_\theta \pi(s_t) |_{\theta=\theta_k}]. \quad (17)$$

(17) can also be rewritten as:

$$\theta_{k+1} = \Gamma_\Theta [\theta_k + \beta_2(k) (-\nabla_\theta \mathcal{L}(\theta, \xi) |_{\theta=\theta_k} + \delta\theta_{k+1} + \delta\theta_\epsilon)].$$

where

$$\begin{aligned} \delta\theta_{k+1} &= \mathbb{E}_{s \sim \mathcal{D}} [\nabla_a (-Q(s, a; \omega_k) + \lambda(s; \xi_k) Q_h(s, a; \phi_k)) |_{a=\pi(s; \theta_k)} \nabla_\theta \pi(s; \theta) |_{\theta=\theta_k}] \\ &\quad - \nabla_a (-Q_{\omega_k}(s_t, a) + \lambda_\xi(s_t) Q_h(s_t, a; \phi_k)) |_{a=a_t} \cdot \nabla_\theta \pi(s_t) |_{\theta=\theta_k} \end{aligned}$$

and

$$\begin{aligned} \delta\theta_\epsilon &= \mathbb{E}_{s \sim \mathcal{D}} [-\nabla_a (-Q(s, a; \omega_k) + \lambda(s; \xi_k) Q_h(s, a; \phi_k)) |_{a=\pi(s; \theta_k)} \nabla_\theta \pi(s; \theta) |_{\theta=\theta_k} \\ &\quad + \nabla_a (-Q^{\pi_{\theta_k}}(s, a) + \lambda(s; \xi_k) Q_h^{\pi_{\theta_k}}(s, a)) |_{a=\pi(s; \theta_k)} \nabla_\theta \pi(s; \theta) |_{\theta=\theta_k}] \end{aligned}$$

1. We will show that $\delta\theta_{k+1}$ is square integrable first, specifically,

$$\mathbb{E}[\|\delta\theta_{k+1}\|^2 \mid \mathcal{F}_{\theta,k}] \leq 2 \cdot [\|\nabla_{\theta}\pi_{\theta}(s)|_{\theta=\theta_k}\|_{\infty}^2 \times (\|\nabla_a Q(s, a; \omega_k)\|_{\infty}^2 + \|\lambda(s; \xi_k)\|_{\infty}^2 \cdot \|\nabla_a Q_h(s, a; \phi_k)\|_{\infty}^2)].$$

Assumption 5.3 implies that

$$\begin{aligned} \|\nabla_{\theta}\pi_{\theta}(s)|_{\theta=\theta_k}\|_{\infty}^2 &\leq K_1(1 + \|\theta_k\|_{\infty}^2), \\ \|\nabla_a Q(s, a; \omega_k)\|_{\infty}^2 &\leq K_2(1 + \max_{a \in \mathcal{A}} \|a\|_{\infty}^2), \\ \|\nabla_a Q_h(s, a; \phi_k)\|_{\infty}^2 &\leq K_3(1 + \max_{a \in \mathcal{A}} \|a\|_{\infty}^2). \end{aligned}$$

where K_1, K_2, K_3 is three sufficiently large scalars. Furthermore, $\lambda(s; \xi_k)$ can be bounded by λ_{max} because $s \in \mathcal{S}_f$. Because of the aforementioned conditions, we can conclude that $\mathbb{E}[\|\delta\theta_{k+1}\|^2 \mid \mathcal{F}_{\theta,k}] \leq 2K_1(1 + \|\theta_k\|_{\infty}^2)[K_2(1 + \max_{a \in \mathcal{A}} \|a\|_{\infty}^2) + \lambda_{max}(K_3(1 + \max_{a \in \mathcal{A}} \|a\|_{\infty}^2))] < \infty$. Thus $\delta\theta_{k+1}$ is square integrable.

2. Second, we will show $\delta\theta_{\epsilon} \rightarrow 0$. Specifically,

$$\begin{aligned} \delta\theta_{\epsilon} &= \mathbb{E}_{s \sim \mathcal{D}}[\nabla_a(-Q^{\pi_{\theta_k}}(s, a) + Q(s, a; \omega_k) + \lambda(s; \xi_k)(Q_h^{\pi_{\theta_k}}(s, a) - Q_h(s, a; \phi_k)))|_{a=\pi(s; \theta_k)} \nabla_{\theta}\pi(s; \theta)|_{\theta=\theta_k}] \\ &= \mathbb{E}_{s \sim \mathcal{D}}[\nabla_a(-Q(s, a; \omega^*) + Q(s, a; \omega_k) + \lambda(s; \xi_k)(Q_h(s, a; \phi^*) - Q_h(s, a; \phi_k)))|_{a=\pi(s; \theta_k)} \nabla_{\theta}\pi(s; \theta)|_{\theta=\theta_k}] \\ &\leq \mathbb{E}_{s \sim \mathcal{D}}[\nabla_{\theta}\pi(s; \theta)|_{\theta=\theta_k}] \cdot (K_4\|\omega_k - \omega^*\|_{\infty} + \lambda_{max}K_5\|\phi_k - \phi^*\|_{\infty}) \rightarrow 0 \end{aligned}$$

where K_4, K_5 is the Lipschitz constant. The limit comes from the convergence of the parameters in **Time scale 1**.

3. Because $\hat{\nabla}_{\theta}\mathcal{J}_{\pi}(\theta)|_{\theta=\theta_k}$ is a sample of $\nabla_{\theta}\mathcal{L}(\theta, \xi)|_{\theta=\theta_k}$, we can conclude that $\mathbb{E}[\delta\theta_{k+1} \mid \mathcal{F}_{\theta,k}] = 0$, where $\mathcal{F}_{\theta,k} = \sigma(\theta_m, \delta\theta_m, m \leq k)$ is the filtration generated by different independent trajectories (Chow et al., 2017).

Based on the three facts, the θ -update given by (17) is a stochastic approximation of the continuous system $\theta(t)$ (Borkar, 2009), described by an ODE:

$$\dot{\theta} = \Upsilon_{\theta}[-\nabla_{\theta}\mathcal{L}(\theta, \lambda)], \quad (18)$$

where

$$\Upsilon_{\theta}[F(\theta)] \triangleq \lim_{\eta \rightarrow 0^+} \frac{\Gamma_{\Theta}(\theta + \eta F(\theta)) - \Gamma_{\Theta}(\theta)}{\eta}$$

is the left directional derivative of the function $\Gamma_{\Theta}(\theta)$ in the direction of $F(\theta)$. The purpose of the directional derivative is to guarantee the update $\Upsilon_{\theta}[-\nabla_{\theta}\mathcal{L}(\theta, \lambda)]$ will point in the descent direction along the boundary of Θ when the θ -update hits the boundary. By invoking the Step 2 in (Chow et al., 2017, Appendix A.2), one can know that $d\mathcal{L}(\theta, \xi)/dt = -\nabla_{\theta}\mathcal{L}(\theta, \lambda)^T \cdot \Upsilon_{\theta}[-\nabla_{\theta}\mathcal{L}(\theta, \lambda)] \leq 0$ and the value will be non-zero if $\|\Upsilon_{\theta}[-\nabla_{\theta}\mathcal{L}(\theta, \lambda)]\| \neq 0$.

Let us consider the continuous system. For a given ξ , define a Lyapunov function

$$L_{\xi}(\theta) = \mathcal{L}(\theta, \xi) - \mathcal{L}(\theta^*, \xi)$$

where θ^* is a local minimum point. Therefore, there exists a scalar r such that $\forall \theta \in B_r(\theta^*) = \{\theta \mid \|\theta - \theta^*\| \leq r\}$, $L_{\xi}(\theta) \geq 0$. Moreover, according to (Bertsekas, 2016, Proposition 1.1.1), we obtain $\Upsilon_{\theta}[-\nabla_{\theta}\mathcal{L}(\theta, \lambda)]|_{\theta=\theta^*} = 0$, which means θ^* is a stationary point. Due to the non-positive property of $d\mathcal{L}(\theta, \xi)/dt$ and refer to the (Khalil & Grizzle, 2002, Chapter 4), aforementioned contents show that for any given initial condition $\theta \in B_r(\theta^*)$, the continuous trajectory of $\theta(t)$ of (18) converges to θ^* , i.e. $\mathcal{L}(\theta^*, \xi) \leq \mathcal{L}(\theta(t), \xi) \leq \mathcal{L}(\theta(0), \xi)$ for $\forall t \geq 0$.

Finally, because of the following properties:

1. From (Chow et al., 2017, Proposition 17), $\nabla_{\theta}\mathcal{L}(\theta, \xi)$ is a Lipschitz function in θ ;
2. The step size schedules follow Assumption 5.4;
3. $\delta\theta_{k+1}$ is a square Martingale difference sequence and $\delta\theta_{\epsilon}$ is a vanishing error;
4. $\theta_k \in \Theta$, which implies that $\sup_k \|\theta_k\| < \infty$ almost surely,

one can invoke (Borkar, 2009, Theorem 2, Chapter 6) (multi-time scale stochastic approximation theory) to know that the sequence $\{\theta_k\}$, $\theta_k \in \Theta$ converges almost surely to the solution of (18), which further converges almost surely to the locally minimum point θ^* .

Time scale 3 (Convergence of ξ -update) The parameter ξ of multiplier is on the slowest time scale so we can assume that during the ξ -update, the policy has converged to the local minimum point, i.e. $\|\theta_k - \theta^*(\xi_k)\| = 0$ and the safety value has converged to a fixed quantity such that $\|Q_h(s, a; \phi_k) - Q_h^{\pi_{\theta^*}}(s, a)\| = 0$. With the continuity of $\nabla_{\xi} \mathcal{L}(\theta, \xi)$, we have $\|\nabla_{\xi} \mathcal{L}(\theta, \xi)|_{\theta=\theta_k, \xi=\xi_k} - \nabla_{\xi} \mathcal{L}(\theta, \xi)|_{\theta=\theta^*(\xi_k), \xi=\xi_k}\| = 0$ almost surely. Thus, the ξ -update can be expressed as:

$$\begin{aligned}\xi_{k+1} &= \Gamma_{\Xi}(\xi_k + \beta_3(k) Q_h(s_t, \pi_{\theta_k}(s_t); \phi_k) \nabla_{\xi} \lambda(s_t)|_{\xi=\xi_k}) \\ &= \Gamma_{\Xi}(\xi_k + \beta_3(k) (\nabla_{\xi} \mathcal{L}(\theta, \xi)|_{\theta=\theta^*(\xi_k), \xi=\xi_k} + \delta\xi_{k+1}))\end{aligned}\quad (19)$$

where

$$\begin{aligned}\delta\xi_{k+1} &= -\nabla_{\xi} \mathcal{L}(\theta, \xi)|_{\theta=\theta^*(\xi_k), \xi=\xi_k} + Q_h(s_t, \pi_{\theta_k}(s_t); \phi_k) \nabla_{\xi} \lambda(s_t)|_{\xi=\xi_k} \\ &= -\mathbb{E}_{s \sim \mathcal{D}}[Q_h^{\pi_{\theta^*}}(s, \pi_{\theta^*}(s)) \nabla_{\xi} \lambda(s; \xi)|_{\xi=\xi_k}] + Q_h(s_t, \pi_{\theta_k}(s_t); \phi_k) \nabla_{\xi} \lambda(s_t)|_{\xi=\xi_k} \\ &= -\mathbb{E}_{s \sim \mathcal{D}}[Q_h^{\pi_{\theta^*}}(s, \pi_{\theta^*}(s)) \nabla_{\xi} \lambda(s; \xi)|_{\xi=\xi_k}] + \\ &\quad (Q_h(s_t, \pi_{\theta_k}(s_t); \phi_k) - Q_h^{\pi_{\theta^*}}(s_t, \pi_{\theta^*}(s_t)) + Q_h^{\pi_{\theta^*}}(s_t, \pi_{\theta^*}(s_t))) \nabla_{\xi} \lambda(s_t)|_{\xi=\xi_k}.\end{aligned}$$

Similar with θ -update, we need to prove the followings:

1. $\delta\xi_{k+1}$ is square integrable because

$$\mathbb{E}[\|\delta\xi_{k+1}\|^2 | \mathcal{F}_{\xi, k}] \leq 2 \frac{r_{max}^2}{(1-\gamma)^2} K_6 (1 + \|\xi_k\|_{\infty}^2) < \infty$$

where K_6 is a sufficiently large number.

2. Since $\|Q_h(s_t, \pi_{\theta}(s_t); \phi_k) - Q_h^{\pi_{\theta^*}}(s_t, \pi_{\theta^*}(s_t))\|_{\infty} \rightarrow 0$ and $Q_h^{\pi_{\theta^*}}(s_t, \pi_{\theta^*}(s_t)) \nabla_{\xi} \lambda(s_t)|_{\xi=\xi_k}$ is sample of $\nabla_{\xi} \mathcal{L}(\theta, \xi)|_{\theta=\theta^*(\xi_k), \xi=\xi_k}$, one can conclude that $\mathbb{E}[\delta\xi_{k+1} | \mathcal{F}_{\xi, k}] = 0$ almost surely, where $\mathcal{F}_{\xi, k} = \sigma(\xi_m, \delta\xi_m, m \leq k)$ is the filtration of ξ generated by different independent trajectories.

Therefore, the ξ -update is a stochastic approximation of the continuous system

$$\dot{\xi} = \Upsilon_{\Xi}[\nabla_{\xi} \mathcal{L}(\theta, \xi)|_{\theta=\theta^*(\xi)}] \quad (20)$$

with a Martingale difference error $\delta\xi_k$, where Υ_{Ξ} is the left directional derivative similarly defined in **Time scale 2**. Analogous to **Time scale 2** and in (Chow et al., 2017, Appendix B.2), $d\mathcal{L}(\theta^*(\xi), \xi)/dt = \nabla_{\xi} \mathcal{L}(\theta, \xi)|_{\theta=\theta^*(\xi)}^T \cdot \Upsilon_{\Xi}[\nabla_{\xi} \mathcal{L}(\theta, \xi)|_{\theta=\theta^*(\xi)}] \geq 0$, which is non-zero if $\|\Upsilon_{\Xi}[\nabla_{\xi} \mathcal{L}(\theta, \xi)|_{\theta=\theta^*(\xi)}]\| \neq 0$.

For a local maximum point ξ^* , define a Lyapunov function

$$L(\xi) = \mathcal{L}(\theta^*(\xi), \xi^*) - \mathcal{L}(\theta^*(\xi), \xi).$$

There exists a scalar r' such that for $\forall \xi \in B_{r'}(\xi^*) = \{\xi \in \Xi \mid \|\xi - \xi^*\| \leq r'\}$, $L(\xi) \geq 0$. Moreover, $dL(\xi(t))/dt = -d\mathcal{L}(\theta^*(\xi), \xi)/dt \leq 0$ and the equal only holds when $\Upsilon_{\Xi}[\nabla_{\xi} \mathcal{L}(\theta, \xi)|_{\theta=\theta^*(\xi)}] = 0$. This means ξ^* is a stationary point. One can invoke (Khalil & Grizzle, 2002, Chapter 4) and conclude that given any initial condition $\xi \in B_{r'}(\xi^*)$, the trajectory of (20) converges to ξ^* , which is a locally maximum point.

Now with (1) $\{\xi_k\}$ is a stochastic approximation to $\xi(t)$ with a Martingale difference error; (2) the step size schedules in Assumption 5.4; (3) the convex and compact property in projection and (4) $\nabla_{\xi} \mathcal{L}(\theta^*(\xi), \xi)$ is a Lipschitz function in ξ . we can apply the multi-time scale stochastic approximation theory again and show that $\{\xi_k\}$ converges to a local maximum point ξ^* almost surely, i.e. $\mathcal{L}(\theta^*(\xi^*), \xi^*) \geq \mathcal{L}(\theta^*(\xi), \xi)$.

Local Saddle Point. From **Time scale 2** and **3** we know that $\mathcal{L}(\theta^*(\xi^*), \xi^*) \geq \mathcal{L}(\theta^*(\xi), \xi)$ and $\mathcal{L}(\theta^*, \xi) \leq \mathcal{L}(\theta, \xi)$. Thus, $\mathcal{L}(\theta^*, \xi) \leq \mathcal{L}(\theta^*, \xi^*) \leq \mathcal{L}(\theta, \xi^*)$, which means (θ^*, ξ^*) is a local saddle point of $\mathcal{L}(\theta, \xi)$. With the saddle point theorem (Bertsekas, 2016, Proposition 5.1.6), we finally come to the conclusion that $\pi(\theta^*)$ is a local optimal policy to the RCRL problem (4).

C. Implementation Details of Algorithms

C.1. The Gap between Assumptions and Practical Implementations

Finite MDP. The boundness of \mathcal{S} , \mathcal{A} , and reward function can be guaranteed in common RL tasks. However, it is in most of the cases that \mathcal{S} and \mathcal{A} are continuous such that they are infinite. One can discretize the space to get a finite one at the cost of inaccuracy but we will keep the space continuous.

Parameterized approximation. A popular choice of function approximators is deep neural networks (NN) that is differentiable in its parameters. However, the general conclusion about the continuity and Lipschitz constant of a NN is still an open problem (Kim et al., 2021). We still adopt NN in our experiments and leverage clipped gradient update (Zhang et al., 2020) as the projection operator to keep the parameters of NNs in compact sets as mentioned in Section 4.3. Moreover, a Lagrange multiplier network introduced by (Ma et al., 2021b) is used for statewise constraint-satisfaction.

Step sizes. Actually we cannot make any schedule of learning rates to make their sum goes to infinity due to a limited number of steps but the sum of the square of learning rates are finite. Furthermore, we utilize $\beta_1(k) > \beta_2(k) > \beta_3(k), \forall k$ to approximate the relationships among the learning rates.

Exploration issue for deterministic policies. Deterministic policies may lack exploration due to overestimation error (Lillicrap et al., 2016; Fujimoto et al., 2018) but this can be mitigated by off-policy updates with a replay buffer, where the learning and the exploration is treated independently. Hence, we construct a stochastic policy giving means and variances of a multivariate Gaussian distribution but only take the means during evaluation.

C.2. Off-policy Parts

Implementation details about off-policy RL algorithms compared in safe-control-gym are covered in this section. For fair comparison, all methods are implemented under the same code base, see (Guan et al., 2021a). The only differences among them is the constrained function and some hyperparameters, which will be explained in detail in the following content.

C.2.1. ALGORITHMS

RAC implementation is similar to common off-policy Lagrangian-based CRL methods but with a different constrained function, i.e. the safety value function. As shown in Algorithm 1, at each update step gradients of the critic, the safety value function, the actor and the multiplier are computed through samples collected from the environment. The actor is updated on an intermediate frequency and the multiplier at the slowest frequency, correspond to Assumption 5.4.

SAC-Lagrangian is a SAC-based implementation of RCPO (Tessler et al., 2019). The constraint imposed on the RL problem is $\mathcal{J}_c^\pi = \mathbb{E}_{s \sim \mathcal{D}, a \sim \pi}[Q_c^\pi(s, a)] \leq \eta$, where $Q_c^\pi(s, a) = \sum_t \gamma^t c(s_t | s_0 = s, a_0 = a, \pi)$ and η is the constraint threshold. Due to the constraint is about expectation rather than statewise, the multiplier λ is a scalar here, but updated with dual ascent similarly with (9).

SAC-Reward Shaping is a SAC-based implementation of fixed penalty optimization (FPO) mentioned in (Achiam et al., 2017; Tessler et al., 2019). It only adds an additional term in the reward function to punish constrain violation, without any constrained optimization approaches. The reward function during training is modified into $r'(s, a) = r(s, a) - \rho h(s)$, where $\rho > 0$ is a fixed penalty coefficient. Then the networks are updated through standard RL and here SAC. Choosing an appropriate ρ is engineering-intuitive and sometimes the tuning process will be time-consuming.

SAC-CBF is inspired by CBF for safe control in control community (Dawson et al., 2021; Ma et al., 2021a; Choi et al., 2021). The core idea is to make potential unsafe behaviors smooth out exponentially as the agent approaches the safe boundary. The constrained function is called barrier function $B(s, a) \triangleq \dot{h}(s) + \mu h(s) \leq 0$ where $\mu \in (0, 1)$ is a hyperparameter.

SAC-SI leverages a human-designed safe index (SI) as the energy function. The control policy needs to keep the system energy low ($\varphi \leq 0$) and dissipate the energy when the system is at high energy ($\varphi > 0$) (Ma et al., 2021c). Hence, the constraint is $\Delta(s, a) \triangleq \varphi(s') - \max\{\varphi(x) - \eta_D, 0\} \leq 0$, where η_D is a slack variable controlling the decent rate of SI. A commonly used SI is in the form of $\varphi(s) = \sigma - (-h(s))^n + k\dot{h}(s)$ (Zhao et al., 2021), which is chosen in this paper.

C.2.2. HYPERPARAMETERS

Table 1 shows the hyperparameters of algorithms evaluated in safe-control-gym.

Table 1. Off-policy Algorithms Hyperparameters in safe-control-gym

Parameter	Value
<i>Shared</i>	
Optimizer	Adam ($\beta_1 = 0.99, \beta_2 = 0.999$)
Approximation function	Multi-layer Perceptron
Number of hidden layers	2
Number of neurons in a hidden layer	256
Nonlinearity of hidden layer	ELU
Nonlinearity of output layer of multiplier	Softplus
Critic/Constrained function learning rate	Linear annealing $1e-4 \rightarrow 1e-6$
Actor learning rate	Linear annealing $2e-5 \rightarrow 1e-6$
Temperature coefficient α learning rate	Linear annealing $8e-5 \rightarrow 8e-6$
Reward discount factor (γ)	0.99
Policy update interval (m_π)	4
Multiplier ascent interval (m_λ)	12
Target smoothing coefficient (τ)	0.005
Max episode length (N)	360
Expected Entropy ($\bar{\mathcal{H}}$)	-2
Replay buffer size	50,000
Replay batch size	512
<i>RAC</i>	
Multiplier learning rate	Linear annealing $6e-7 \rightarrow 1e-7$
<i>SAC-Lagrangian</i>	
Multiplier learning rate	$3e-4$
<i>SAC-SI</i>	
Multiplier learning rate	Linear annealing $1e-6 \rightarrow 1e-7$
σ, n, k	0.1, 2, 1
η_D	0.1
<i>SAC-CBF</i>	
Multiplier learning rate	Linear annealing $1e-6 \rightarrow 1e-7$
μ	0.1
<i>SAC-Reward Shaping</i>	
Critic learning rate	Linear annealing $3e-5 \rightarrow 3e-6$
Actor learning rate	Linear annealing $8e-5 \rightarrow 8e-6$
Policy update interval (m_π)	1
ρ	0.5

C.3. On-policy Parts

Implementation details about on-policy RL algorithms including the on-policy version of RCRL benchmarked in Safety-Gym are covered in this section. For fair comparison, all methods are implemented under the same code base, see (Achiam & Amodei, 2019).

C.3.1. ALGORITHMS

RCO. The advantages function for reward value and safety value are denoted as A^π and A_h^π . Denote policy parameterization as π_θ , the loss function of RCO when policy parameters, $\theta = \theta_k$ is

$$\mathcal{J}(\theta, \xi) = \mathbb{E}_{s, a \sim \pi_{\theta_k}} \left\{ \overline{A^{\pi_{\theta_k}}}(s, a) + \lambda_\xi(s) \overline{A_h^{\pi_{\theta_k}}}(s, a) \right\} \quad (21)$$

where

$$\overline{A^{\pi_{\theta_k}}}(s, a) = \min \left(\frac{\pi_{\theta_k}(a | s)}{\pi_{\theta_k}(a | s)} A^{\pi_{\theta_k}}(s, a), g(\epsilon, A^{\pi_{\theta_k}}(s, a)) \right), \quad g(\epsilon, A) = \begin{cases} (1 + \epsilon)A & A \geq 0 \\ (1 - \epsilon)A & A < 0 \end{cases}$$

$\overline{A_h^{\pi_{\theta}}}(s, a)$ has a similar computation.

Algorithm 2 Reachable Constrained Optimization (RCO)

Require: Initial policy parameters θ_0 , value and cost value function parameters ω_0, ϕ_0 , multiplier network parameters ξ_0

- 1: **for** $k = 0, 1, 2, \dots$ **do**
 - 2: Collect set of trajectories $\mathcal{D}_k = \{\tau_i\}$ with policy π_{θ_k} , where τ_i is a T -step episode.
 - 3: Compute reward-to-go $\hat{R}_t \doteq \sum_{i=t}^T \gamma^i r_i$ and cost-to-go $\hat{H}_t \doteq \max_t h_t$.
 - 4: Compute advantage functions $A^{\pi_{\theta_k}}, A_h^{\pi_{\theta_k}}$, according to the value function V_{ω_k} and cost value function $V_{h_{\phi_k}}$. Compute the multiplier λ_{ξ} .
 - 5: Update the policy parameters θ by minimizing (21)
 - 6: Update the multiplier parameters ξ by maximizing (21)
 - 7: Fit value function, cost value function by regression on mean-square error
 - 8: **end for**
-

PPO-CBF, PPO-SI. Constraint functions of these baselines are the same as the off-policy version, only the base algorithm is replaced with PPO (Schulman et al., 2017). Compared with Algorithm 2, only the computation of cost-to-go changes to the energy-function-based versions.

Table 2. Detailed hyperparameters of on-policy algorithm and baselines.

Algorithm	Value
<i>Shared</i>	
Optimizer	Adam ($\beta_1 = 0.9, \beta_2 = 0.999$)
Approximation function	Multi-layer Perceptron
Number of hidden layers	2
Number of hidden units per layer	64
Nonlinearity of hidden layer	ELU
Nonlinearity of output layer (other than multiplier net)	linear
Critic learning rate	Linear annealing $3e-4 \rightarrow 0$
Reward discount factor (γ)	0.99
Cost discount factor (γ_c)	0.99
GAE parameters	0.95
Batch size	8000
Max episode length (N)	1000
Actor learning rate	Linear annealing $3e-4 \rightarrow 0$
Clip ratio	0.2
KL margin	1.2
<i>RCO, PPO-CBF, PPO-SI</i>	
Nonlinearity of output layer, multiplier net	softplus
Multiplier learning rate	Linear annealing $1e-4 \rightarrow 0$
<i>PPO-Lagrangian</i>	
Init λ	$0.268(\text{softplus}(0))$
<i>PPO-SI</i>	
σ, n, k	0.1, 2, 1
<i>PPO-CBF</i>	
μ	0.1

C.3.2. HYPERPARAMETERS

See Table 2.

D. Details about Experiments

D.1. Quadrotor Trajectory Tracking in safe-control-gym

Details about the quadrotor trajectory tracking task and training will be covered in this section. The task for the quadrotor is to track a counter-clockwise circle trajectory as accurately as possible while keeping its altitude z between $[0.5, 1.5]$, meaning the lower and upper bound of a tunnel. Note that only the next waypoint is accessible to the quadrotor at each time step, so no planning or predictive control in advance exists in this task.

Elements of the RL setting. The state space $\mathcal{S} \subset \mathbb{R}^{12}$ consists of the current state of the quadrotor $\mathbf{x} = [x, \dot{x}, z, \dot{z}, \theta, \dot{\theta}]^T$ and the information of the next waypoint \mathbf{x}^{ref} , thus $s_t = [\mathbf{x}_t; \mathbf{x}_t^{ref}]$. The action is the thrusts given by the two motors on both sides $[T_1, T_2]$, whose value will be normalized to $[0, 1] \times [0, 1]$. The system dynamics and information about the whole trajectory is inaccessible to the agent. The circle center is at $(0, 1)$ and its radius is 1. The circle is discretized into 360 points so at each time step the reward function is the weighted sum of the difference between (\mathbf{x}, a) and the reference $(\mathbf{x}^{ref}, a^{ref})$, specifically, $r(s_t, a_t) = (\mathbf{x}_t - \mathbf{x}_t^{ref})^T Q (\mathbf{x}_t - \mathbf{x}_t^{ref}) + (a_t - a_t^{ref})^T R (a_t - a_t^{ref})$ where $Q = \text{diag}(10, 1, 10, 1, 0.2, 0.2)$, $R = \text{diag}(1e-4, 1e-4)$. The constraint is $0.5 \leq z \leq 1.5$.

Initialization. For better exploration and generality of the learned feasible set and policy, we initialize the quadrotor uniformly in a rectangle in the xz -plane with uniformly distributed vertical and horizontal speed, pitch angle and pitch angle rate, specific ranges in Table 3. The nearest discrete waypoint on the trajectory to the initial location of the quadrotor is assigned as the start waypoint. In other words, the start waypoints change as the initial location changes. Quadrotor initialized at the center will be assigned a start waypoint randomly.

Table 3. The Initialization Range of Each Variable

Variable	Range
x	$[-1.5, +1.5]$
\dot{x}	$[-1.0, +1.0]$
z	$[0.25, +1.75]$
\dot{z}	$[-1.5, +1.5]$
θ	$[-0.2, +0.2]$
$\dot{\theta}$	$[-0.1, +0.1]$

Training. At each time step, the quadrotor outputs the two torques based on its state, including the waypoint next to the one in the last time step in the counter-clockwise direction. Then it receives the state transition, the reward and constraint function or cost signal. The (s, a, r, s', h, c) will be sent to the replay buffer. Simultaneously, the learner gets batches of samples from the replay buffer and compute gradients to update the function approximators. The maximum length T of an episode equals to the number of the discrete waypoints, i.e. 360. The episode will be ended and reset when the maximum length is reached or the quadrotor flies out of the bound ($|x| > 2$ or $|z| > 3$).

Evaluation. The policy is evaluated for four runs at one time. It is initialized statically at $(1, 1)$, $(-1, 1)$, $(0, 0.53)$, $(0, 1.47)$ respectively in a run where safety can be guaranteed by hovering so the four initial states are feasible. Then the average of the return $\sum_{t=0}^{T-1} r(s_t, a_t)$ and constraint violation rate $\frac{\sum_{t=0}^{T-1} c(s_t)}{T}$ are taken as the performance and constraint-satisfaction metrics.

Feasible sets projection. The approximated constrained function in each algorithm ($Q_h^\pi(s, a)$, $B^\pi(s, a)$, $\Delta(s, a)$ in RAC, SAC-CBF, SAC-SI, respectively) is a function $f : \mathbb{R}^{12} \mapsto \mathbb{R}$. Hence, we need to project the high-dimensional state to a lower one to visualize the constrained function. Because the imposed constraints is about the z -coordinate, we choose to project each state onto the xz -plane and observe the changing trend with varying \dot{z} . Coordinates in x - and z -axis are uniformly sampled from the set $\{(x, z) \mid |x| < 1.5, 0.5 < z < 1.5\}$ while \dot{z} is chosen among $\{-1, 0, 1\}$ and \dot{x} , θ and $\dot{\theta}$ are all set to zero. The tracking waypoint of each sample is the nearest one on the circle trajectory to the (x, z) sample. Then we generate state s for a given (x, z) tuple according to the aforementioned rules and get action a from the trained policy. The constrained value can be calculated with $f(s, a)$.